Theoretical study of the addition of alkyl and halogenoalkyl radicals to the ethylene double bond: a comparison between Hartree–Fock, perturbation theory and density functional theory

Andrea Bottoni

Dipartimento di Chimica 'G. Ciamician', Universita' di Bologna, via Selmi 2, 40126 Bologna, Italy

The addition reactions of the radicals $^{\bullet}CH_3$, $^{\bullet}CH_2CH_3$, $^{\bullet}CH(CH_3)_2$, $^{\bullet}C(CH_3)_3$, $^{\bullet}CH_2F$, $^{\bullet}CF_3$ and $^{\bullet}CCl_3$ to the ethylene double bond have been investigated using traditional *ab initio* methods (UHF, CASSCF, MP2 and MP4) and density functional theory (DFT). The DFT computations have been performed with different functionals including in all cases non-local corrections. At all levels of theory we have located for each reaction one or two transition states. When two transition states exist they correspond to different conformers which are always very close in energy. The computations have shown that the geometries of the various transition states are not very sensitive to the nature of the attacking radical. The most relevant change is a decrease in the reactant-like character of the transition state with the increasing nucleophilic character of the attacking radical. The various results also show that the topology of the reaction surface is satisfactorily described at the UHF level and that the geometries are not dramatically affected by the correlation energy corrections which cause only an increase in the reactant-like character of the transition states. However, the inclusion of dynamic correlation is essential to obtain reasonable values of the computed activation energies. We have found that the energy barriers computed with the DFT approach are strongly dependent on the type of functional which is used. The best values are provided by the Becke's three parameter hybrid functional (B3LYP). In this case the computed activation energies are in better agreement with experiment than the corresponding MP2 and MP4 values (the difference between the computed and the experimental values is in all cases within 1 kcal mol^{-1}†). The present study indicates the B3LYP functional as a satisfactory calibration of DFT methods suitable for investigating extensively this class of reaction.

Introduction

The radical addition to double bonds has received a great deal of attention from both the experimental[1,2] and theoretical[3] point of view. These reactions are in fact recognized as a powerful method for intermolecular bond formation and represent the central reaction in many polymer processes. Several mechanistic studies over the last two decades have shown that the rate and the orientation of free radical addition to olefins are the results of a 'complex interplay of polar, steric and bond-strength factors.'[1a] Giese and Tedder in two comprehensive review articles have presented an analysis of polar and steric effects.[2] Tedder in particular[2a] has proposed five useful rules to be used to establish the relative importance of these factors in specific cases. Nevertheless it seems that no simple property can be used to provide a general qualitative theory which is capable of predicting the course of these reactions. To this purpose the computational approach can be of great help and the recent progress of computational chemistry has made possible the study of such a problem using advanced methods which have already provided useful information on the transition-state structure, the regioselectivity and the activation barriers and enthalpies for this type of reactions.[3]

In this paper we focus our attention on the addition of alkyl radicals and halogenoalkyl radicals to the ethylene double bond, *e.g.*, reaction (1), where $^{\bullet}R$ = $^{\bullet}CH_3$, $^{\bullet}C_2H_5$, $^{\bullet}CH(CH_3)_2$, $^{\bullet}C(CH_3)_3$, $^{\bullet}CH_2F$, $^{\bullet}CF_3$ and $^{\bullet}CCl_3$, and we investigate from a theoretical point of view the change in the reaction parameters (mainly activation energies and transition state geometries) associated with the variation in the attacking radical $^{\bullet}R$. Since carbon-centred radicals are nucleophilic or electrophilic species depending upon the substituent at the radical center, the above series contains examples of both types of radicals: electron donating substituents like alkyl groups increase the nucleophilicity whereas electron-withdrawing substituents augment the electrophilic character. These radical reactions are particularly suitable for a theoretical investigation since they have been experimentally studied in the gas phase.[4] Thus the activation parameters which have been determined are not modified by the solvation effects and can be compared directly with the theoretical values. These experimental results show in particular that the substitution of the hydrogen atoms of a methyl radical with alkyl groups has only a small effect on the reaction rate. The rate regularly decreases (and the activation barriers only slightly increase or remain constant) on passing from the methyl radical to the more branched alkyl radicals, but the variations are very small and are always within possible experimental error. On the other hand the inclusion of polar substituents, like fluorine or chlorine, has a more substantial effect and the reaction rates (and the corresponding activation barriers) vary significantly compared with the methyl radical.

$$^{\bullet}R + H_2C{=}CH_2 \longrightarrow \text{products} \qquad (1)$$

To investigate these reactions we use the unrestricted Hartree–Fock (UHF) method and the Møller–Plesset perturbation theory up to second (MP2) and fourth order (MP4) and in a few cases we compute also the CASSCF wave-function to check the reliability of a single-reference approach. It is well known that the HF method is capable of providing reasonable geometrical parameters for the most part of stable organic molecules and in many cases (if a single configuration is dominant), also for the transition states, whereas the

† 1 cal = 4.184 J.

frequencies computed at this level of theory are in general too large and the activation barriers are usually overestimated. On the other hand the application of *ab initio* methods including dynamic correlation (like MP2 and MP4) improves greatly the description and provides, for example, barriers in good agreement with the experiment. However, since the cost of correlated *ab initio* methods is high and increases rapidly with the increasing size of the molecules, their application is still limited to rather small systems.

In the last decade much interest has been given to methods based on density functional theory (DFT)[5] which appeared as a versatile computational approach capable of describing successfully many problems previously covered exclusively by *ab initio* HF and post-HF methods. DFT-based methods have been applied to many types of structural and reactivity problems using, in particular, the form which is known as local density approximation (LDA).[6] These studies have shown that local methods provide geometries which are in better agreement with experiment than the HF results (in particular for transition metal complexes)[7] even if unsatisfactory results have been found in the calculation of energy barriers and bond energies which are systematically overestimated.[7j] Many of the problems of the local approaches have been eliminated introducing correction terms based on electron density gradients (non-local methods).[8] These corrections added to the functional improve the evaluation of the exchange and correlation terms and provide much better results in the computation of bond energies and in the description of metal–metal and metal–ligand bonds.

Since in recent years only a few papers have appeared where a systematic comparison between traditional correlated *ab initio* methods and DFT-based methods has been carried out,[7i-k] we have applied different forms of non-local DFT methods to the study of the title reactions. Our purpose is to compare the accuracy of DFT techniques with post-HF methods (like MP2 and MP4) in computing molecular properties. A calibration of DFT methods for identifying strengths and weaknesses of each functional is nowadays particularly important since this approach has become recently quite popular. This popularity stems in large measure from its computational expedience which makes DFT-based methods particularly suitable for the computations on large molecular systems.

Computational procedure

All the DFT and *ab initio* molecular computations reported here were performed with the Gaussian 92/DFT[9] series of programs using the 6-31G* basis set.[10] In all cases (HF, MP2, CASSCF and DFT) the geometries of the various critical points were fully optimized with the gradient method available in Gaussian 92. The nature of each critical point was characterized by computing the harmonic vibrational frequencies. To obtain a better estimation of the contribution of the dynamic correlation, additional single point energy calculations based on the MP2 optimized geometries were carried out at the full MP4SDTQ level. As suggested by Sosa and Schlegel[11] we used spin-projected energies to cancel the spin contamination which affects the transition structures and which can cause an overestimation of the energy barriers.

For the DFT computations we have used two pure and two hybrid functionals as implemented in Gaussian 92/DFT. Following the Gaussian 92/DFT formalism, these functionals can be written as expression (2) where $E(S)_x$ is the Slater

$$a_1E(S)_x + a_2E(HF)_x + a_3E(B88)_x + a_4E(LOCAL)_c + a_5E(NON\text{-}LOCAL)_c \quad (2)$$

exchange,[6a,b] $E(HF)_x$ is the Hartree–Fock exchange, $E(B88)_x$ is the Becke's 1988 non-local exchange functional corrections,[8h] $E(LOCAL)_c$ is a local correlation functional and $E(NON\text{-}LOCAL)_c$ is the gradient-corrected correlation functional. One of the two hybrid functionals that we have used corresponds to the Becke's three-parameter exchange functional[8l] and is denoted here as B3LYP. In this case, $E(LOCAL)_c$ corresponds to the Vosko, Wilk and Nusair (VWN) local correlation functional[6d] and $E(NON\text{-}LOCAL)_c$ to the correlation functional of Lee, Yang and Parr (LYP)[8f,i] which includes both local and non-local terms; the coefficients in expression (2) are those determined by Becke ($a_1 = 0.80$, $a_2 = 0.20$, $a_3 = 0.72$, $a_4 = 0.19$ and $a_5 = 0.81$). The other hybrid method, denoted here as BHLYP, is characterized by the following parameters: $a_1 = 0.50$, $a_2 = 0.50$, $a_3 = 0.50$, $a_4 = 0.00$ and $a_5 = 1.00$.

The two pure DFT functionals differ only in the correlation term. The functional denoted as BLYP is given in expression (3)

$$E(S)_x + E(B88)_x + E(LYP)_c \quad (3)$$

while that denoted as BP86 is given by expression (4) where

$$E(S)_x + E(B88)_x + E(P86)_c \quad (4)$$

$E(P86)_c$ includes both the local functional of Perdew[6e] and his gradient corrections.[8d]

To verify the validity of the HF and MP2 approaches in describing the transition state region we investigated the potential energy surfaces for the reactions involving the $^{\bullet}CH_3$, $^{\bullet}CH_2CH_3$ and $^{\bullet}CH_2F$ radicals at the CASSCF level of theory. The active space used in these computations is that required to describe correctly the formation of the new C–C σ bond and the simultaneous breaking of the C–C π bond. It consists of three electrons in three orbitals, *i.e.* the π (doubly occupied) and the π* (empty) orbitals associated with the C–C olefin bond, and the singly occupied pσ orbital associated with the non-bonding electron of the alkyl and halogenoalkyl radicals.

Results and discussion

The 6-31G* transition structures located for the addition of $^{\bullet}CH_3$, $^{\bullet}CH_2CH_3$ and $^{\bullet}CH(CH_3)_2$ radicals to ethylene are shown in Fig. 1, while those located for the addition of $^{\bullet}C(CH_3)_3$, $^{\bullet}CH_2F$, $^{\bullet}CF_3$ and $^{\bullet}CCl_3$ are represented in Fig. 2. The most relevant geometrical parameters are collected in Tables 1–7. The bond lengths and bond angles given in these tables are defined in the structure shown below and also in the two figures. The energies of reactants and transition structures are given in Table 8. In this table we have also reported the values of the experimental activation energies ($E_{a,exp.}$) and those of the computed activation energies (E_a) which include the zero-point vibrational energy corrections (ZPE). The MP4 activation

Table 1 Transition-state optimized geometries[a] for the reaction $^{\bullet}CH_3 + C_2H_4$ obtained with the 6-31G* basis set at various levels of theory

	HF	CAS	MP2	BHLYP	B3LYP	BLYP	BP86
r	2.245	2.245	2.261	2.310	2.363	2.423	2.473
a	1.382	1.378	1.344	1.351	1.356	1.364	1.358
b	1.076	1.076	1.082	1.077	1.084	1.091	1.092
c	1.076	1.076	1.082	1.077	1.084	1.091	1.092
d	1.077	1.077	1.084	1.078	1.086	1.093	1.093
∠*ra*	109.1	109.8	109.6	109.4	109.8	110.3	110.3
∠*rb*	102.7	103.2	101.8	101.0	100.1	99.3	98.0
∠*rc*	102.7	103.2	101.8	101.0	100.1	99.3	98.0
∠*rd*	100.9	101.9	100.1	99.6	99.4	99.1	98.2
∠*bc*	115.6	115.1	116.1	116.5	116.9	117.3	117.8
∠*cd*	115.7	115.3	116.4	116.8	117.2	117.6	118.2
∠*bd*	115.7	115.3	116.4	116.8	117.2	117.6	118.2
ω	180.0	180.0	180.0	180.0	180.0	180.0	180.0
ε	158.2	156.8	163.1	163.7	164.8	165.5	167.9
φ	174.3	172.1	175.9	176.4	176.6	176.6	177.2

[a] Bond lengths are in Ångstroms and angles in degrees.

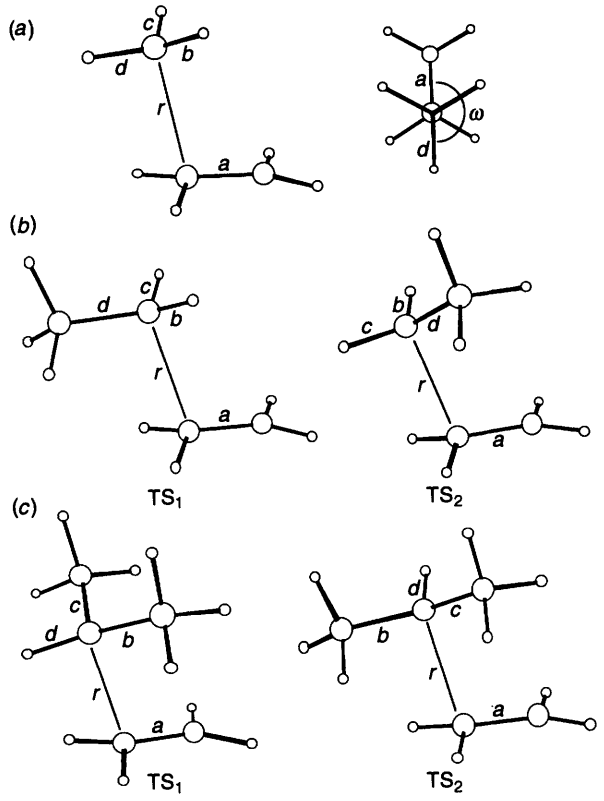

Fig. 1 Transition-state structures corresponding to the addition of (*a*) the $^{\bullet}CH_3$ radical (*b*) the $^{\bullet}CH_2CH_3$ radical (*c*) and of the $^{\bullet}CH(CH_3)_2$ radical to the ethylene double bond

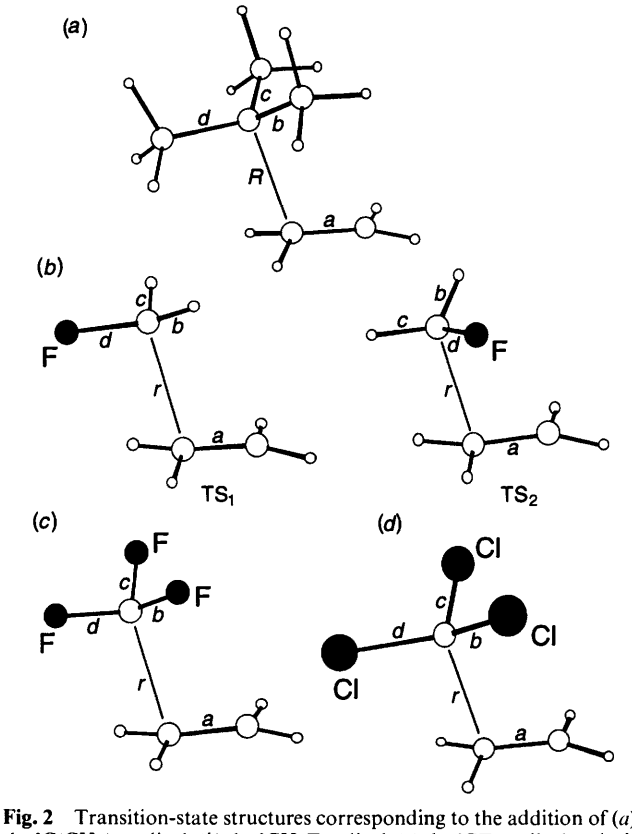

Fig. 2 Transition-state structures corresponding to the addition of (*a*) the $^{\bullet}C(CH_3)_3$ radical, (*b*) the $^{\bullet}CH_2F$ radical, (*c*) the $^{\bullet}CF_3$ radical and (*d*) the $^{\bullet}CCl_3$ radical to the ethylene double bond

energies were computed using the ZPE values obtained at the MP2 level.

The geometry of the transition state for the addition of $^{\bullet}CH_3$ to ethylene is shown in Fig. 1(*a*). This structure has already been determined at the UHF level by Houk *et al.*[3f] with the 3-21G basis set and by Schlegel *et al.*[3j] with the more accurate 6-31G* basis set. For comparison we also report in Table 1 the UHF/6-31G* results and we discuss them briefly. At this level of theory the forming C–C bond and the breaking C=C double bond are, respectively, 2.245 and 1.382 Å, while the angle of attack of the radical to the alkene is 109.1°. As a consequence of the formation of the new C–C bond a considerable rehybridization of the olefin carbon atom C_1 takes place. A measure of the pyramidalization of C_1 is given by the angle ε which is 158.2° (where ε corresponds to the angle between the C=C olefinic bond and the bisector of the HC_1H angle; its value is 180° in the planar ethylene). The two methylenic hydrogens bonded to C_2 are only slightly bent out of the ethylene molecular plane but in the opposite direction with respect to C_1: the pyramidalization of C_2 is described by the φ angle which is 174.3°. These results

Table 2 Transition-state optimized geometries[a] for the reaction $^{\bullet}C_2H_5 + C_2H_4$ obtained with the 6-31G* basis set at various levels of theory

	HF	CAS	MP2	BHLYP	B3LYP	BLYP	BP86
TS_1							
r	2.232	2.234	2.256	2.288	2.334	2.384	2.433
a	1.383	1.379	1.344	1.353	1.358	1.367	1.361
b	1.078	1.078	1.085	1.079	1.087	1.094	1.095
c	1.078	1.078	1.085	1.079	1.087	1.094	1.095
d	1.507	1.508	1.499	1.493	1.498	1.504	1.497
∠*ra*	109.9	110.8	111.0	110.9	111.6	112.2	112.5
∠*rb*	100.6	101.1	99.6	98.7	97.7	97.0	95.8
∠*rc*	100.6	101.1	99.6	98.7	97.7	97.0	95.8
∠*rd*	105.9	106.4	104.6	104.7	104.9	105.2	104.3
∠*bc*	113.3	112.9	113.9	114.2	114.4	114.6	115.1
∠*cd*	116.6	116.3	117.4	117.8	118.2	118.4	119.0
∠*bd*	116.6	116.3	117.4	117.8	118.2	118.4	119.0
ω	180.0	180.0	180.0	180.0	180.0	180.0	180.0
ε	157.0	155.8	162.7	162.4	162.9	163.1	165.8
φ	174.2	172.3	175.9	176.0	176.3	176.1	176.5
TS_2							
r	2.227		2.254	2.286	2.333	2.383	2.435
a	1.383		1.344	1.353	1.358	1.367	1.361
b	1.078		1.086	1.079	1.087	1.094	1.095
c	1.079		1.087	1.080	1.089	1.096	1.097
d	1.505		1.496	1.491	1.496	1.502	1.495
∠*ra*	110.0		110.0	110.2	110.8	111.3	110.9
∠*rb*	100.4		99.3	98.5	97.4	96.5	94.8
∠*rc*	98.5		98.4	97.2	96.8	96.4	96.1
∠*rd*	108.1		105.8	106.3	106.2	106.2	104.9
∠*bc*	113.4		114.1	114.4	114.6	114.8	115.4
∠*cd*	116.6		117.7	117.9	118.3	118.1	118.6
∠*bd*	116.4		117.1	117.5	117.8	118.6	119.3
ω	60.8		55.2	56.2	56.2	55.9	55.7
ε	156.9		162.8	162.4	163.0	163.3	166.2
φ	174.4		176.2	176.4	176.4	176.3	177.1

[a] Bond lengths are in Ångstroms and angles in degrees.

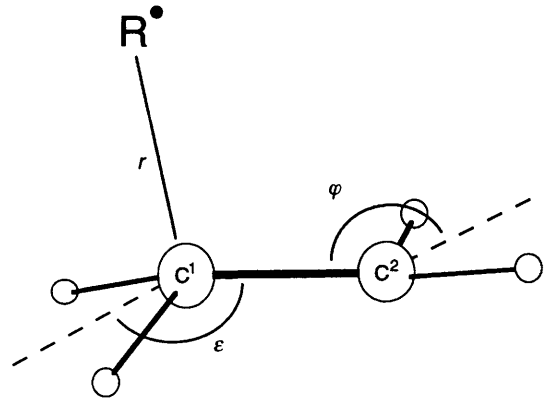

Table 3 Transition-state optimized geometries[a] for the reaction $^{\bullet}CH(CH_3)_2 + C_2H_4$ obtained with the 6-31G* basis set at various levels of theory

	HF	MP2	BHLYP	B3LYP	BLYP	BP86
TS_1						
r	2.210	2.249	2.265	2.305	2.344	2.399
a	1.385	1.343	1.355	1.361	1.371	1.364
b	1.507	1.497	1.494	1.500	1.508	1.500
c	1.507	1.497	1.494	1.500	1.508	1.500
d	1.081	1.090	1.082	1.091	1.098	1.099
∠*ra*	110.7	110.3	110.8	111.4	111.9	111.4
∠*rb*	106.0	104.1	104.4	104.0	103.8	102.7
∠*rc*	106.0	104.1	104.4	104.0	103.8	102.7
∠*rd*	96.6	96.0	95.0	94.3	93.8	92.9
∠*bc*	116.6	117.3	117.6	118.1	118.4	118.8
∠*cd*	114.4	115.6	115.6	115.8	115.9	116.6
∠*bd*	114.4	115.6	115.6	115.8	115.9	116.6
ω	180.0	180.0	180.0	180.0	180.0	180.0
ε	155.5	162.6	161.0	161.3	160.8	164.1
φ	174.5	176.4	176.0	176.1	176.1	176.8
TS_2						
r	2.215	2.250	2.267	2.307	2.345	2.399
a	1.385	1.343	1.355	1.361	1.371	1.364
b	1.508	1.499	1.495	1.501	1.508	1.501
c	1.507	1.497	1.493	1.499	1.507	1.499
d	1.080	1.088	1.081	1.090	1.097	1.098
∠*ra*	110.8	111.3	111.5	112.0	112.5	112.3
∠*rb*	103.6	102.9	102.5	102.8	102.9	102.3
∠*rc*	106.2	104.4	104.9	104.5	104.5	103.3
∠*rd*	98.8	97.2	96.3	94.9	94.0	92.6
∠*bc*	116.9	117.8	118.2	118.7	119.0	119.6
∠*cd*	114.2	115.1	115.2	115.3	115.4	116.0
∠*bd*	114.4	115.3	115.4	115.6	115.7	116.4
ω	59.5	64.7	64.7	61.9	64.8	65.8
ε	155.8	162.5	161.0	161.1	160.9	164.5
φ	174.3	176.3	176.2	172.2	175.9	176.8

[a] Bond lengths are in Ångstroms and angles in degrees.

Table 4 Transition-state optimized geometries[a] for the reaction $^{\bullet}C(CH_3)_3 + C_2H_4$ obtained with the 6-31G* basis set at various levels of theory

	HF	MP2	BHLYP	B3LYP	BLYP	BP86
r	2.200	2.249	2.250	2.280	2.305	2.361
a	1.387	1.343	1.357	1.365	1.375	1.367
b	1.511	1.499	1.498	1.505	1.515	1.506
c	1.511	1.499	1.498	1.505	1.515	1.506
d	1.512	1.500	1.499	1.506	1.515	1.507
∠*ra*	111.6	111.4	111.9	109.2	112.9	112.4
∠*rb*	104.5	102.6	102.8	102.4	102.2	101.0
∠*rc*	104.5	102.6	102.8	102.4	102.2	101.0
∠*rd*	102.0	101.2	100.7	100.7	100.8	100.1
∠*bc*	114.5	115.5	115.4	115.6	115.7	116.3
∠*cd*	114.7	115.9	115.8	116.0	116.1	116.8
∠*bd*	114.7	115.9	115.8	116.0	116.1	116.8
ω	180.0	180.0	180.0	180.0	180.0	180.0
ε	154.2	162.3	159.6	159.0	158.2	161.8
φ	174.4	176.5	175.8	176.0	175.6	176.5

[a] Bond lengths are in Ångstroms and angles in degrees.

Table 5 Transition-state optimized geometries[a] for the reaction $^{\bullet}CH_2F + C_2H_4$ obtained with the 6-31G* basis set at various levels of theory

	HF	CAS	MP2	BHLYP	B3LYP	BLYP	BP86
TS_1							
r	2.242	2.241	2.250	2.299	2.355	2.419	2.484
a	1.379	1.376	1.343	1.350	1.355	1.363	1.358
b	1.075	1.076	1.085	1.078	1.088	1.095	1.096
c	1.075	1.076	1.085	1.078	1.088	1.095	1.096
d	1.343	1.344	1.364	1.341	1.352	1.365	1.357
∠*ra*	110.3	110.9	111.5	111.5	111.7	111.9	111.6
∠*rb*	104.8	105.2	104.2	103.5	102.2	101.2	99.4
∠*rc*	104.8	105.2	104.2	103.5	102.2	101.2	99.4
∠*rd*	103.8	104.5	103.0	102.7	104.3	105.4	106.7
∠*bc*	117.3	116.7	118.1	118.6	118.9	119.3	120.1
∠*cd*	112.2	112.0	112.6	113.0	113.3	113.4	113.9
∠*bd*	112.2	112.0	112.6	113.0	113.3	113.4	113.9
ω	180.0	180.0	180.0	180.0	180.0	180.0	180.0
ε	159.8	160.4	164.2	164.4	165.1	165.7	168.3
φ	175.6	173.6	176.8	176.9	177.0	176.9	177.6
TS_2							
r	2.248		2.251	2.293	2.344	2.402	2.462
a	1.379		1.343	1.351	1.356	1.364	1.359
b	1.075		1.085	1.078	1.087	1.095	1.096
c	1.077		1.087	1.080	1.090	1.097	1.098
d	1.341		1.362	1.340	1.351	1.364	1.365
∠*ra*	107.9		108.6	110.1	110.9	111.5	111.5
∠*rb*	105.0		105.0	104.2	102.8	101.8	99.8
∠*rc*	103.4		104.0	102.2	101.5	101.1	100.6
∠*rd*	105.4		103.0	104.1	105.2	106.0	106.3
∠*bc*	117.3		118.0	118.4	118.7	119.1	119.9
∠*cd*	112.1		112.3	112.7	112.9	113.1	113.5
∠*bd*	112.2		112.6	113.0	113.3	113.4	113.8
ω	60.7		68.7	80.4	82.7	84.2	85.9
ε	159.2		163.8	163.7	164.4	164.9	167.5
φ	174.2		175.9	176.4	176.5	176.5	177.2

[a] Bond lengths are in Ångstroms and angles in degrees.

Table 6 Transition-state optimized geometries[a] for the reaction $^{\bullet}CF_3 + C_2H_4$ obtained with the 6-31G* basis set at various levels of theory

	HF	MP2	BHLYP	B3LYP	BLYP	BP86
r	2.299	2.291	2.374	2.442	2.535	2.689
a	1.372	1.338	1.343	1.349	1.356	1.349
b	1.307	1.335	1.314	1.332	1.350	1.342
c	1.307	1.335	1.314	1.332	1.350	1.342
d	1.310	1.340	1.318	1.335	1.354	1.346
∠*ra*	106.6	105.9	105.5	105.7	105.2	105.2
∠*rb*	109.4	109.0	108.5	108.1	108.0	107.2
∠*rc*	107.8	109.0	108.5	108.1	108.0	107.2
∠*rd*	102.0	109.2	109.1	110.0	110.5	111.1
∠*bc*	110.1	110.0	110.2	110.2	110.1	110.4
∠*cd*	110.0	109.9	110.2	110.2	110.1	110.4
∠*bd*	110.0	109.9	110.2	110.2	110.1	110.4
ω	180.0	180.0	180.0	180.0	180.0	180.0
ε	163.3	167.7	168.6	169.4	170.6	174.2
φ	176.1	177.3	177.6	177.7	177.6	178.7

[a] Bond lengths are in Ångstroms and angles in degrees.

are very similar to those obtained with the smaller 3-21G basis suggesting that bond lengths and angles are not very sensitive to the basis set.

For the addition reactions involving the ethyl radical and the isopropyl radical we have located two transition states [Fig. 1(*b*) and 1(*c*) and Tables 2 and 3, respectively], which are very close in energy as is evident from the values reported in Table 8 which will be discussed later in detail. One transition state (TS_1) has in both cases a C_s symmetry: for $^{\bullet}R = {}^{\bullet}CH_2CH_3$, the terminal methyl group is *anti* and the two C–H bonds are staggered with respect to the C=C double bond, while for $^{\bullet}R = {}^{\bullet}CH(CH_3)_2$ the two terminal methyl groups are in a staggered arrangement and the C–H bond is *anti* with respect to the olefinic bond. The other transition state (TS_2) corresponds to a *gauche* arrangement of the terminal methyl group ($^{\bullet}R = {}^{\bullet}CH_2CH_3$) or of the C–H bond [$^{\bullet}R = {}^{\bullet}CH(CH_3)_2$] with respect to the C=C double bond. The two different conformational situations corresponding to TS_1 and TS_2 are described by the dihedral angle ω which is 180° in the *anti* orientation and about 60° in the *gauche* orientation at the UHF level [ω is defined by the two planes *dr* and *ra* and is shown in Fig. 1(*a*) for $^{\bullet}CH_3$]. A similar situation has been found for $^{\bullet}CH_2F$. Also in this case two different transition states exist [Fig. 2(*b*) and Table 5]: they again have similar energy and correspond to an *anti* (TS_1 with C_s symmetry) and to a *gauche* (TS_2) arrangement of the C–F bond with respect to the olefinic bond. For $^{\bullet}C(CH_3)_3$, $^{\bullet}CF_3$ and $^{\bullet}CCl_3$ [see Figs. 2(*a*), (*c*) and (*d*)

Table 7 Transition-state optimized geometries[a] for the reaction $^{\bullet}CCl_3 + C_2H_4$ obtained with the 6-31G* basis set at various levels of theory

	HF	MP2	BHLYP	B3LYP	BLYP	BP86
r	2.199	2.238	2.237	2.266	2.296	2.362
a	1.383	1.342	1.355	1.362	1.371	1.363
b	1.740	1.736	1.739	1.761	1.788	1.765
c	1.740	1.736	1.739	1.761	1.788	1.765
d	1.743	1.740	1.743	1.766	1.796	1.772
∠*ra*	108.4	107.4	108.3	109.2	108.8	109.5
∠*rb*	106.7	106.1	106.3	106.7	107.3	106.3
∠*rc*	106.7	106.1	106.3	106.7	107.3	106.3
∠*rd*	103.1	102.9	102.8	103.0	103.4	102.5
∠*bc*	113.3	113.7	113.6	113.3	112.8	113.6
∠*cd*	113.1	113.4	113.6	113.1	112.6	113.4
∠*bd*	113.1	113.4	113.4	113.1	112.6	113.4
ω	180.0	180.0	180.0	180.0	180.0	180.0
ε	158.0	164.7	162.5	162.7	162.5	165.8
φ	175.0	176.4	176.2	176.2	176.1	176.8

[a] Bond lengths are in Ångstroms and angles in degrees.

and Tables 4, 6 and 7, respectively] we have located a transition state which has the same C_s symmetry as the transition state found for the methyl radical: in all cases it is characterized by a staggered arrangement of the radical C–C, C–F or C–Cl bonds with respect to the C=C double bond. For all the transition structures that we have located we have computed the corresponding hessian matrix which, at all levels of theory, is characterized by a negative eigenvalue. The corresponding eigenvector is dominated by the approaching distance *r*.

At all computational levels we have found that the geometries of the various transition states are not very sensitive to the nature of the attacking radical $^{\bullet}R$. We discuss first briefly the UHF results and then we analyse the geometrical modifications found using perturbation theory or the DFT approach. In all cases a significant rehybridization of the carbon atom C_1, similar to that observed for CH_3, occurs as is evident from the values of the angle ε. This angle slightly decreases on passing from the methyl radical (158.2°) to the ethyl (157.0° and 156.9°), isopropyl (155.5° and 155.8°) and *tert*-butyl (154.2°) radical showing that the pyramidalization of C_1 increases in the same direction. The change in the radical $^{\bullet}R$ is also responsible for the variation in the length of the new forming C–C bond *r* which decreases along the series $^{\bullet}CH_3$, $^{\bullet}CH_2CH_3$, $^{\bullet}CH(CH_3)_2$ and $^{\bullet}C(CH_3)_3$ [the corresponding values of the *r* distance at the UHF level are 2.245 Å for $^{\bullet}CH_3$, 2.232 and 2.227 Å for $^{\bullet}CH_2CH_3$, 2.210 and 2.215 Å for $^{\bullet}CH(CH_3)_2$, 2.200 Å for $^{\bullet}C(CH_3)_3$]. Thus the trend in ε and *r* shows that the reactant-like character of the transition state decreases with the increase in the nucleophilic character of the attacking radical. On the other hand the *r* distance changes only slightly when only one of the three methyl hydrogens are replaced by a fluorine atom (*r* = 2.242 and 2.248 Å for $^{\bullet}CH_2F$), but increases significantly for $^{\bullet}CF_3$ (*r* = 2.299 Å) and decreases for $^{\bullet}CCl_3$ (*r* = 2.199 Å). Also the ε angle changes slightly for R = $^{\bullet}CH_2F$ (159.8° and 159.2°) and for $^{\bullet}CCl_3$ (158.0°), but increases for $^{\bullet}CF_3$ becoming 163.3°.

The other important geometrical parameter which should be discussed is the angle ∠*ra* which characterizes the radical attack. Our results show that this parameter does not change very much with the increasing size of the attacking alkyl radical: this angle in fact only slightly increases in the direction $^{\bullet}CH_3$ (109.1°) < $^{\bullet}CH_2CH_3$ (109.9° and 110.0°) < $^{\bullet}CH(CH_3)_2$ (110.7° and 110.8°) < $^{\bullet}C(CH_3)_3$ (111.6°). However, it changes more significantly when the halogen substitution on the radical carbon atom increases and becomes 107.9° in the *gauche* transition state found for $^{\bullet}CH_2F$, 106.6° for $^{\bullet}CF_3$ and 108.8° for $^{\bullet}CCl_3$.

A point of interest in our computations concerns the adequacy of the UHF level of theory in describing the transition state region for these reactions. Tables 1, 2 and 5 contain the values of the salient geometrical parameters computed at the CASSCF level for $^{\bullet}CH_3$ and the two *anti* transition states found for $^{\bullet}CH_2CH_3$ and $^{\bullet}CH_2F$. These values are seen to be very similar to those obtained at the UHF level. This result is in agreement with the composition of the CASSCF wavefunction which is dominated by the SCF configuration (the weight of this configuration is 0.954, 0.954 and 0.953 for $^{\bullet}CH_3$, $^{\bullet}CH_2CH_3$ and $^{\bullet}CH_2F$, respectively) and demonstrates that the effect of the non-dynamic correlation is negligible and that a single configuration can satisfactorily describe the potential energy surface of this class of reactions.

The inclusion of the dynamic correlation (MP2 and MP4 levels) has the effect of making the *r* distance longer and the C=C double bond *a* shorter: for $^{\bullet}CH_3$, for example, *r* varies from 2.245 to 2.261 Å and *a* varies from 1.382 to 1.344 Å. Similar changes have been found for the other radicals. The dynamic correlation also has the effect of decreasing slightly the angles ∠*rb*, ∠*rc* and ∠*rd* (the attacking radical becomes more planar) and the pyramidalization of the carbon atom C_1 as shown by the values of the angle ε which increases in all cases. Thus the MP2 computations predict earlier transition structures than the UHF method. A more significant geometry change due to the dynamic correlation has been found in the ω angle which characterizes the *gauche* transition states: for $^{\bullet}CH_2CH_3$, $^{\bullet}CH(CH_3)_2$ and $^{\bullet}CH_2F$ this angle becomes 55.2, 64.7 and 68.7°, respectively, at the MP2 level. It is interesting to point out that the inclusion of the dynamic correlation does not change the trend in the various geometrical parameters associated with the change in the nature of the attacking radical.

The MP2 geometries compare rather well with the geometries obtained at different levels of density functional theory. The most important changes found with DFT are a further lengthening of the *r* distance, a further decrease in the ∠*rb*, ∠*rc* and ∠*rd* angles and an increase in the angle ε (the carbon C_1 becomes less pyramidal) with a consequent increase in the reactant-like character of the transition states. These changes are moderate when hybrid DFT methods are used (BHLYP and B3LYP), but become more important with pure DFT methods like BLYP and BP86, *e.g.* for the methyl radical *r* is 2.310 and 2.363 Å at the BHLYP and B3LYP levels, respectively, but becomes 2.423 Å with the BLYP functional and 2.473 Å with the BP86 functional; similarly ε is 163.7 and 164.8° at the BHLYP and B3LYP levels, but becomes 165.5 and 167.9° at the BLYP and BP86 levels. Another significant structural change has been found in the ω angle which, for example in the case of $^{\bullet}R = {}^{\bullet}CH_2F$, becomes greater than 80°. Also at the DFT level of theory the trend in the geometrical parameters as a function of the nature of the radical $^{\bullet}R$ is the same as that determined with the UHF method.

The accurate prediction of the energy barriers of radical reactions is a difficult problem and it is well known that high levels of theory including dynamic correlation are needed to reproduce the experimental results.[11] Thus it is not surprising that the activation barriers obtained at the UHF level and CASSCF level are in all cases overestimated. A large decrease in the energy barriers is observed when the projected MP2 approach is used. These projected barriers compare better with the experimental values even if in two cases ($^{\bullet}CH_3$ and $^{\bullet}CH_2F$) they are still overestimated and for $^{\bullet}C(CH_3)_3$, $^{\bullet}CF_3$ and $^{\bullet}CCl_3$ they are quite underestimated: the computed values for $^{\bullet}CH_3$ and $^{\bullet}CH_2F$ are in fact 8.9 and 6.6 kcal mol^{-1}, respectively, which should be compared with 6.8 and 4.3 kcal mol^{-1}, while the computed barriers for $^{\bullet}C(CH_3)_3$, $^{\bullet}CF_3$ and $^{\bullet}CCl_3$ are 4.6, 1.2 and 4.1 kcal mol^{-1}, respectively, which must be compared with the experimental values of 7.1, 2.4 and 6.3 kcal mol^{-1}. Furthermore the computed activation energy decreases along the series $^{\bullet}CH_3$, $^{\bullet}CH_2CH_3$, $^{\bullet}CH(CH_3)_2$, $^{\bullet}C(CH_3)_3$ in disagreement with the experimental values which remain almost constant. Also the trend obtained in the comparison between

Table 8 Transition-state energies (E)[a,b] relative to reactants and activation energies (E_a)[a] computed for the radical addition reaction $^{\bullet}R + C_2H_4$ with the 6-31G* basis set at various levels of theory; for each reaction the experimentally available activation energy ($E_{a,exp}$)[a] is reported

	HF	CAS	MP2	MP4	BHLYP	B3LYP	BLYP	BP86
R = $^{\bullet}CH_3$ ($E_{a,exp.}$ = 7.3 kcal mol^{-1})[c]								
E	9.42	13.51	5.77	6.71	5.94	4.38	3.15	2.18
E_a	11.6	16.3	8.9	9.8	8.2	6.6	5.2	4.1
R = $^{\bullet}CH_2CH_3$ ($E_{a,exp.}$ = 6.9 kcal mol^{-1})[d]								
TS_1								
E	10.08	14.15	5.11	6.17	6.58	5.15	4.01	2.81
E_a	11.5	16.6	7.6	8.7	8.5	7.2	5.9	4.7
TS_2								
E	9.96	—	4.76	5.84	6.34	4.97	3.89	2.67
E_a	11.5	—	7.4	8.4	8.4	7.0	5.8	4.3
R = $^{\bullet}CH(CH_3)_2$ ($E_{a,exp.}$ = 6.9 kcal mol^{-1})[d]								
TS_1								
E	10.55	—	3.67	4.92	6.64	5.47	4.60	3.08
E_a	11.8	—	5.9	7.2	8.5	7.5	6.6	4.9
TS_2								
E	10.64	—	3.97	5.19	6.79	5.53	4.56	3.06
E_a	11.8	—	6.2	7.4	8.8	7.7	6.7	5.1
R = $^{\bullet}C(CH_3)_3$ ($E_{a,exp.}$ = 7.1 kcal mol^{-1})[d]								
E	11.61	—	2.65	4.08	7.07	6.17	5.52	3.60
E_a	12.5	—	4.6	6.0	8.7	8.0	7.4	5.3
R = $^{\bullet}CH_2F$ ($E_{a,exp.}$ = 4.3 kcal mol^{-1})[e]								
TS_1								
E	7.67	11.95	3.98	4.91	4.76	3.25	2.25	1.29
E_a	8.6	13.5	6.1	7.0	6.3	4.3	3.7	2.7
TS_2								
E	8.28	—	4.60	5.52	5.34	3.76	2.69	1.72
E_a	9.1	—	6.6	7.4	6.8	5.1	4.2	3.1
R = $^{\bullet}CF_3$ ($E_{a,exp.}$ = 2.4 kcal mol^{-1})[f]								
E	4.31	—	0.26	0.95	1.44	0.45	0.42	0.63
E_a	4.5	—	1.2	1.9	1.9	1.0	1.0	1.1
R = $^{\bullet}CCl_3$ ($E_{a,exp.}$ = 6.3 kcal mol^{-1})[g]								
E	9.98	—	2.78	4.30	6.68	5.59	4.55	2.89
E_a	10.1	—	4.1	5.1	7.4	6.4	5.3	3.6

[a] Values in kcal mol^{-1}. [b] The absolute energy values (atomic units) for reactants are as follows: R = $^{\bullet}CH_3$ −117.590 71(HF), −117.615 01(CAS), −117.955 77(MP2), −118.010 40(MP4), −118.339 41(BHLYP), −118.425 74(B3LYP), −118.342 50(BLYP), −118.410 57(BP86); R = $^{\bullet}CH_2CH_3$ −156.628 87(HF), −156.653 14(CAS), −157.122 74(MP2), −157.193 53(MP4), −157.631 70(BHLYP), −157.745 34(B3LYP), −157.634 83(BLYP), −157.727 80(BP86); R = $^{\bullet}CH(CH_3)_2$ −195.667 85(HF), −196.292 52(MP2), −196.379 29(MP4), −196.924 86(BHLYP), −197.0655 81(B3LYP), −196.927 65(BLYP), −197.045 62(BP86); R = $^{\bullet}C(CH_3)_3$ −234.706 73(HF), −235.464 14(MP2), −235.566 62(MP4), −236.218 08(BHLYP), −236.385 75(B3LYP), −236.220 29(BLYP), −236.363 37(BP86); R = $^{\bullet}CH_2F$ −216.433 83(HF), −216.458 93(CAS), −216.965 97(MP2), −217.023 41(MP4), −217.532 89(BHLYP), −217.651 47(B3LYP), −217.569 24(BLYP), −217.639 00(BP86); R = $^{\bullet}CF_3$ −414.162 90(HF), −415.029 96(MP2), −415.091 23(MP4), −415.957 66(BHLYP), −416.138 47(B3LYP), −416.055 40(BLYP), −416.131 75(BP86); R = $^{\bullet}CCl_3$ −1494.279 88(HF), −1495.036 53(MP2), −1495.127 68(MP4), −1497.088 58(BHLYP), −1497.210 76(B3LYP), −1497.098 07(BLYP), −1497.295 87(BP86). [c] See ref. 4*a*. [d] See ref. 4*b*. [e] See ref. 4*c*. [f] See ref. 4*d*. [g] See ref. 4*e*.

$^{\bullet}C(CH_3)_3$ (4.6 kcal mol^{-1}) and $^{\bullet}CH_2F$ (6.1 kcal mol^{-1}) is in contrast with the experiment which provides 7.1 and 4.4 kcal mol^{-1}, respectively. Note that the MP2 barriers are in better agreement with the experiment than the MP4 values: at this level the overestimation becomes more significant.

The values of the energy barriers provided by the DFT approach varies significantly according to the type of functional which is used. The BHLYP functional still overestimates the activation barriers even if the trend along the series $^{\bullet}CH_3$, $^{\bullet}CH_2CH_3$, $^{\bullet}CH(CH_3)_2$, $^{\bullet}C(CH_3)_3$, $^{\bullet}CH_2F$, $^{\bullet}CF_3$ and $^{\bullet}CCl_3$ is now in much better agreement with the experiment. The same trend has been obtained with the two pure DFT functionals BLYP and BP86, but in these cases the E_a values are underestimated. The best agreement with the experiment is found for the values computed at the B3LYP level of theory. In this case the difference between the experimental and the corresponding computed value is in all cases within 1 kcal mol^{-1} (except for $^{\bullet}CF_3$). The trend in the activation energies obtained when the methyl hydrogen atoms are substituted by alkyl groups or by halogen atoms agrees satisfactorily with that experimentally observed. However, while the experimental barrier only slightly decreases on going from $^{\bullet}CH_3$ to $^{\bullet}CH_2CH_3$, it remains constant for $^{\bullet}CH(CH_3)_2$ and again slightly increases for $^{\bullet}C(CH_3)_3$, the computed barriers regularly increase (6.6, 7.0, 7.5 and 8.0 kcal mol^{-1}) with the increasing size of the attacking radical.

Another point of interest are the conformations of the transition states and their relative energies. For R = $^{\bullet}CH_2CH_3$, the lower energy transition state is represented at all computational levels by the *gauche* structure TS_2; the difference between the two conformations is in all cases within 0.4 kcal mol^{-1}. The only exception is found at the Hartree–Fock level which gives the same energy for TS_1 and TS_2. For $^{\bullet}R$ = $^{\bullet}CH(CH_3)_2$ the C_s structure TS_1, where both methyl groups are staggered with respect to the double bond, is at a lower energy than TS_2. Also here the two structures are degenerate at the Hartree–Fock level. Thus in both cases the most favourable situation is represented by a *gauche* arrangement of the more cumbersome methyl groups with respect to the double bond. For $^{\bullet}CH_2F$ the C_s structure has a lower energy than the *gauche*,

but also in this case the difference between the two conformations is quite small (within 0.5 kcal mol^{-1}). Note that for $^{\bullet}CH_2CH_3$ and $^{\bullet}CH(CH_3)_2$, the inclusion of the dynamic correlation is essential to differentiate the energies of the two conformations.

Conclusions

In this paper we have reported the results of a comprehensive theoretical study of the addition reactions of the radicals $^{\bullet}CH_3$, $^{\bullet}CH_2CH_3$, $^{\bullet}CH(CH_3)_2$, $^{\bullet}C(CH_3)_3$, $^{\bullet}CH_2F$, $^{\bullet}CF_3$ and $^{\bullet}CCl_3$ to the ethylene double bond. The study compares the results of traditional *ab initio* methods (UHF, CASSCF, MP2 and MP4) with those obtained with DFT-based methods and with experiment. For the DFT computations we have used two pure and two hybrid functionals which include in all cases non-local corrections. At all levels of theory we have located for each reaction one or two transition states. When two transition states exist they correspond to different conformers which are always very close in energy. These computations have shown the following. (*i*) Multiconfigurational effects are negligible in this type of reaction and a single-configuration computational scheme can provide a satisfactory description of the topology of the reaction surfaces. (*ii*) The geometries of the various transition states are not very sensitive to the nature of the attacking radical. The most relevant change is a decrease in the reactant-like character of the transition state with the increasing nucleophilic character of the attacking radical. (*iii*) The geometries are not dramatically affected by the inclusion of dynamic correlation corrections: the most significant geometrical changes are associated with the new forming C–C bond, which becomes longer, and the pyramidalization of the carbon C_1 which decreases; these variations indicate an increasing reactant-like character at the MP2 level. (*iv*) The DFT computations provide geometrical results which are quite similar to those obtained at the MP2 level even if the reactant-like character of the transition states increases further; this modification is small at the BHLYP and B3LYP levels (hybrid method) and more significant when pure DFT functionals are used. (*v*) Even if the topology of the surface is satisfactorily described at the UHF level, the inclusion of dynamic correlation for reactants and transition states is essential to obtain reasonable values of the computed activation energies. We have found that the energy barriers computed with the DFT approach are strongly dependent on the type of functional which is used. The best values have been obtained with the hybrid functional B3LYP which, in many cases, provides activation energies which are in better agreement with experiment than the corresponding MP2 and MP4 values (except for $^{\bullet}R = CF_3$ the difference between the computed and the experimental values is in all cases within 1 kcal mol^{-1}).

All these results indicate that DFT-based methods and traditional correlated methods like Møller–Plesset perturbation theory give similar results, even if the DFT approach seems to provide better energetics if a suitable calibration is chosen. The calibration performed here suggests that the B3LYP functional can be used extensively to investigate this class of reaction.

References

1 (*a*) J. M. Tedder and C. Walton, *Acc. Chem. Res.*, 1976, **9**, 183; (*b*) J. M. Tedder and C. Walton, *Adv. Phys. Org. Chem.*, 1978, **51**; (*c*) J. M. Tedder and C. Walton, *Tetrahedron*, 1980, **36**, 701; (*d*) H. R. Dütsch and H. Fischer, *Int. J. Chem. Kinet.*, 1982, **14**, 195; (*e*) K. Münger, and H. Fischer *Int. J. Chem. Kinet.*, 1985, **17**, 811; (*f*) H. Fischer and H. Paul, *Acc. Chem. Res.*, 1987, **20**, 200; (*g*) K. Heberger, M. Walbiner and H. Fischer, *Angew. Chem., Int. Ed. Engl.*, 1992, **31**, 635; (*h*) K. Heberger and H. Fischer, *Int. J. Chem. Kinet*, 1993, **25**, 249.

2 (*a*) J. M. Tedder, *Angew. Chem., Int. Ed. Engl.*, 1982, **21**, 401; (*b*) B. Giese, *Angew. Chem, Int. Ed. Engl.*, 1983, **22**, 753.

3 (*a*) M. J. S. Dewar and S. Olivella, *J. Am. Chem. Soc.*, 1978, **100**, 5290; (*b*) H. B. Schlegel, K. C. Bhalla and W. L. Hase, *J. Phys. Chem.*, 1982, **86**, 4883; (*c*) H. B. Schlegel and C. Sosa, *J. Phys. Chem.*, 1984, **88**, 1141; (*d*) R. Arnaud, R. Subra, V. Barone, F. Lelj, S. Olivella, A. Sole' and N. Russo, *J. Chem. Soc., Perkin. Trans. 2*, 1986, 1517; (*e*) T. Clark, *J. Chem. Soc., Chem. Commun.*, 1986, 1774; (*f*) K. N. Houk, M. N. Paddon-Row, D. C. Spellmeyer, N. G. Rondan and S. Nagase, *J. Org. Chem.*, 1986, **51**, 2874; (*g*) C. Sosa and H. B. Schlegel, *J. Am. Chem. Soc.*, 1987, **109**, 7007; (*h*) C. Sosa and H. B. Schlegel, *J. Am. Chem. Soc.*, 1987, **109**, 4193; (*i*) R. Arnaud, *New. J. Chem.*, 1989, **13**, 543; (*j*) C. Gonzalez, C. Sosa and H. B. Schlegel, *J. Phys. Chem.*, 1989, **93**, 2435; (*k*) H. Zipse, J. He, K. N. Houk and B. Giese, *J. Am. Chem. Soc.*, 1991, **113**, 4324; (*l*) R. Arnaud and S. Vidal, *New. J. Chem.*, 1992, **16**, 471; (*m*) M. W. Wong, A. Pross and L. Radom, *J. Am. Chem. Soc.* 1993, **115**, 11 050; (*n*) M. W. Wong, A. Pross and L. Radom, *J. Am. Chem. Soc.*, 1994, **116**, 11 938; (*o*) M. W. Wong, A. Pross and L. Radom, *J. Am. Chem. Soc.*, 1994, **116**, 6284; (*p*) W. H. Donovan and G. R. Famini, *J. Phys. Chem.*, 1994, **98**, 7811.

4 (*a*) P. M. Holt and J. A. Kerr, *Int. J. Chem. Kinet.*, 1977, **9**, 185; (*b*) J. A. Kerr and F. Trotman-Dickenson, *Progr. React. Kinet.*, 1961, **1**, 107; (*c*) J. M. Sangster and J. C. J. Thynne, *Trans. Faraday Soc.*, 1969, **65**, 2110; (*d*) J. M. Sangster and J. C. J. Thynne, *J. Phys. Chem.*, 1969, **73**, 2746; (*e*) J. M. Tedder and J. C. Walton, *Trans. Faraday Soc.*, 1964, **60**, 1769.

5 R. G. Parr and W. Yang, *Density-Functional Theory of Atoms and Molecules*, Oxford University Press, New York, 1989.

6 (*a*) P. Hohenberg and W. Kohn, *Phys. Rev. B*, 1964, **136**, 864; (*b*) W. Kohn and L. J. Sham, *Phys. Rev. A*, 1965, **140**, 1133; (*c*) O. Gunnarson and I. Lundquist, *Phys. Rev. B*, 1974, **10**, 1319; (*d*) S. H. Vosko, L. Wilk and M. Nusair, *Can. J. Phys.*, 1980, **58**, 1200; (*e*) J. P. Perdew and A. Zunger, *Phys. Rev. B*, 1981, **23**, 5048; (*f*) V. Tschinke and T. Ziegler, *Can. J. Chem.*, 1989, **67**, 460.

7 (*a*) L. Versluis and T. Ziegler, *J. Chem. Phys.*, 1988, **88**, 322; (*b*) F. Lan, L. Versluis. T. Ziegler, E. J. Baerends and W. Ravenek, *Int. J. Quantum Chem.*, 1988, **S22**, 173; (*c*) J. Harris, R. O. Jones and J. E. Muller, *J. Chem. Phys.*, 1981, **75**, 3904; (*d*) R. Fournier, J. Andzelm and D. R. Salahub, *J. Chem. Phys.*, 1989, **90**, 6371; (*e*) B. Delley, *J. Chem. Phys.*, 1991, **94**, 7245; (*f*) D. Hohl, R. O. Jones, R. Car and M. Parrinello, *J. Chem. Phys.*, 1988, **89**, 6823; (*g*) R. O. Jones and D. Hohl, *J. Chem. Phys.*, 1990, **92**, 6710; (*h*) F. Sim, D. R. Salahub and M. Depuis, *J. Chem. Phys.*, 1991, **95**, 6050; (*i*) G. Fitzgerald and J. Andzelm, *J. Phys. Chem.*, 1991, **95**, 10 531; (*j*) T. Ziegler, *Chem. Rev.*, 1991, **91**, 651; (*k*) L. Fan and T. Ziegler, *J. Am. Chem. Soc.*, 1992, **114**, 10 890.

8 (*a*) D. C. Langreth and M. Mehl, *Phys. Rev. B*, 1983, **28**, 1809; (*b*) A. D. Becke, *Int. J. Quantum Chem.*, 1983, **27**, 1915; (*c*) A. D. Becke, *J. Chem. Phys.*, 1986, **84**, 4524; (*d*) J. P. Perdew, *Phys. Rev. B*, 1986, **33**, 8822; (*e*) A. D. Becke, *Phys. Rev. A*, 1988, **33**, 2786; (*f*) C. Lee, W. Yang and R. G. Parr, *Phys. Rev. B*, 1988, **37**, 785; (*g*) A. D. Becke, *Int. J. Quantum Chem.*, 1989, **S23**, 599; (*h*) A. D. Becke, *Phys. Rev. A*, 1988, **38**, 3098; (*i*) A. Miehlich, A. Savin, H. Stoll and H. Preuss, *Chem. Phys. Lett.*, 1989, **157**, 200; (*l*) A. D. Becke, *J. Chem. Phys.*, 1993, **98**, 5648.

9 Gaussian 92/DFT, Revision G.1, M. J. Frisch, G. W. Trucks, H. B. Schlegel, P. M. W. Gill, B. G. Johnson, M. W. Wong, J. B. Foresman, M. A. Robb, M. Head-Gordon, E. S. Replogle, R. Gomperts, J. L. Andres, K. Raghavachari, J. S. Binkley, C. Gonzalez, R. L. Martin, D. J. Fox, D. J. Defrees, J. Baker, J. J. P. Stewart and J. A. Pople, Gaussian, Inc., Pittsburgh PA, 1993.

10 P. C. Hariharan and J. A. Pople, *Theor. Chim. Acta*, 1973, **28**, 213.

11 C. Sosa and H. B. Schlegel, *Int. J. Quantum Chem.*, 1986, **29**, 1001; 1987, **30**, 155.

Paper 5/06077J
Received 14*th September* 1995
Accepted 29*th May* 1996